Identification Design for Dynamic Voltage Restorer to Mitigate Voltage Sag Based on the Elliptical Transformation

Li, Peng; Wang, Yi; Savaghebi, Mehdi; Lu, Jinghang; Pan, Xuewei; Blaabjerg, Frede

Published in:
IEEE Journal of Emerging and Selected Topics in Power Electronics

DOI (link to publication from Publisher):
10.1109/JESTPE.2020.3047151

Publication date:
2021

Document Version
Accepted author manuscript, peer reviewed version

Citation for published version (APA):
Li, P., Wang, Y., Savaghebi, M., Lu, J., Pan, X., & Blaabjerg, F. (2021). Identification Design for Dynamic Voltage Restorer to Mitigate Voltage Sag Based on the Elliptical Transformation. *IEEE Journal of Emerging and Selected Topics in Power Electronics*, *9*(5), 5672 - 5686. Article 9306800. https://doi.org/10.1109/JESTPE.2020.3047151

Identification Design for Dynamic Voltage Restorer to Mitigate Voltage Sag Based on the Elliptical Transformation

Peng Li, Yi Wang, Mehdi Savaghebi, *Senior Member, IEEE,* Jinghang Lu, *Member, IEEE,* Xuewei Pan, *Member, IEEE,* and Frede Blaabjerg, *Fellow, IEEE,*

***Abstract*—In this paper, a new identification tool for dynamic voltage restorer (DVR) is proposed to achieve flexible active and reactive power dispatch during voltage sags. The presented tool entirely relies on the theoretical analysis of the elliptical transformation, and identification marks are determined for different power injections by using one set of digital codes. Besides, two parameters are presented in the accurate mathematical description of the current references, which guarantee continuous power delivery by selecting the proper values. The chief advantages include the smooth transition state during changes in different power deliveries as well as the elimination of active and reactive power oscillations. Then, the characteristics of the identification tool corresponding to the different power dispatch are analyzed to reveal the feasibility of the given current references. Finally, experimental tests utilizing a laboratory prototype are used to verify the flexibility of the proposed control schemes.**

***Index Terms*—Voltage sags, elliptical transformation, identification tool, power dispatch, dynamic voltage restorer, power quality**

I. Introduction

THE widespread use of renewable energy sources has a significant impact on the stability of the distribution system, and puts forward higher requirements for improving power quality during voltage sags [1], [2]. In addition, the industrial production has always acted in compliance with the strict international standards [3], [4], or different national grid codes [5], [6]. As a result, a voltage sag study is essential to predict the effect of the event on sensitive loads and industrial processes. In other words, timely mitigation of voltage sag is understood as the most attractive solution to improve power quality in the distribution system. The preservation of the rated magnitude and the removal of the phase jump should be identified as the criteria when the improvement of power quality is adopted in [7]. At the same time, the introduction of custom power instruments, particularly the use of dynamic voltage restorer (DVR) at the realm of disturbance suppression, has dramatically improved the load power quality to satisfy the industrial production activities. It is also a very economical solution of eliminating voltage sags [8], [9]. Fig.1 shows the diagram of the DVR connected to the sensitive load through the secondary winding of the transformer. In this configuration, the three-phase converter is connected to the primary of the transformer via an LC filter. The required energy can be taken from an energy storage device that is connected to the dc link, which balances the power flow from the DVR to the ac source.

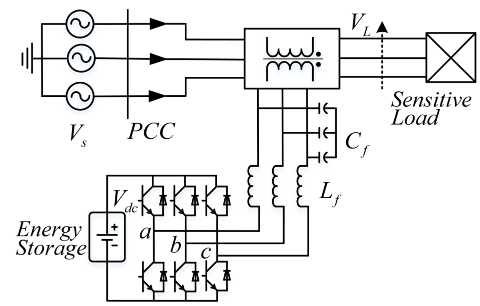

Fig. 1: Circuit diagram of a DVR configuration

In recent studies, the development of compensation strategy for DVR based on the instantaneous reactive power theory [10]–[12] is applied to improve the relevant power quality indicators significantly. An attractive solution, named pre-phase compensation [13], [14], has been proposed where the different voltage sags can be eliminated at the cost of a large number of active power requirements. Other solutions, including in-phase strategy and energy-optimized strategy, have been presented in [15], [16], but the main drawback with these approaches is a failure to eliminate phase jump.

Concerning the control strategies for the mentioned compensation methods, the positive-negative sequence component (PNSC) is an excellent base for the flexible power quality regulation to enhance the DVR's behavior [17]–[19]. Similarly, different control objectives have been presented when alleviating the symptoms of current harmonics [20], [21], dc-

Manuscript received June 22, 2020; revised September 20, 2020 and October 22,2020; accepted November 30, 2020. This work was supported by the China Postdoctoral Science Foundation under Project 2020M681093, and also supported by the Shenzhen Basic Research Project under grant JCYJ20180306172056738. Corresponding author: Jinghang Lu, email: jinghang.lu@ieee.org

Peng Li, Wang Yi, Jinghang Lu and Xuewei Pan are with the School of Mechanical Engineering and Automation, Harbin Institute of Technology, Shenzhen, 518055, China (email: lipengshizhang@163.com; wangyi601@aliyun.com; jinghang.lu@ieee.org; xwpanhit.edu.cn)

M. Savaghebi is with Electrical Engineering Section, the Mads Clausen Institute, University of Southern Denmark, Odense, Denmark (email: mesa@mci.sdu.dk)

Frede Blaabjerg is with the Department of Energy Technology, Aalborg University, Aalborg DK-9220, Denmark. (email: fbl@et.aau.dk)

side ripple [22], [23], overvoltage tripping [24], [25], and peak current limitation [26], [27].

In addition, the power oscillation significantly affects the continuity of the power supply from DVR with exceeding the maximum allowable power capability. Furthermore, advanced controllers for PNSC presented in [28]–[34] can achieve an insightful control objective related to the removal of power oscillations. In [28], the controller only provides active power delivery without the corresponding oscillation term while maintaining the injected voltage safely controlled to a predefined value. In [29], the injection of the peak current can be achieved by delivering only reactive power, and the oscillation elimination of reactive power is a priority objective. Studies [30], [31] deal with the oscillation elimination of active power focused on dc-link voltage optimization, active power exchange maximization, and a combination of the two. Meanwhile, the control strategy in [32] is carried out in order to achieve the oscillation eliminations of active and reactive power simultaneously providing priority to active power delivery to maintain the maximum current injection. Nevertheless, the reference generators of the controller [32] may exceed the current capability of the converter and then lead to the disconnection of the converter due to overcurrent. On the contrary, the control strategy in [33] can restore the dropped voltage magnitudes to the rated values confined within the maximum voltage limit, guaranteeing oscillation elimination of power terms. Specifically, study [34] is conceived to completely avoid power oscillations considering certain specific techniques (e.g. power-characteristic-oriented or voltage-support-oriented) when injecting active and reactive power through sophisticated reference generators. As a drawback, it is unable to maximize power delivery capability. However, control strategies should be optimized according to the load requirements, taking into account not only the maximum power capability of DVR but also the gradual transition process from one power injection level to another. In this sense, the interesting methods based on the elliptical transformation have been presented to maximize the volt-ampere sizing in [35], [36], but they are only the preliminary studies. Therefore, the simple and effective mechanism satisfying the aforementioned gradual transition process needs further investigation.

In this paper, the mentioned elliptical transformation has been used to build a new identification tool that can show the change in the joining regions of different power injection levels. This new property can reflect realistically the dynamic response of DVR by an adjustable active and reactive power dispatch. In detail, this dynamic process is defined as a triplet of the digital codes. Three digits form an identification tool, where the first digit denotes the flexible selection of individual power control strategy, and the last two digits denote the criteria to continuous power delivery based on two control parameters. The values of two parameters change continuously in the fixed numerical ranges and describe the different applications embedded in the elliptical trajectory. In other words, this advantage can prioritize between active and reactive power regulation according to the first digital code, and an easy mechanism of tuning the last two digital codes permits to different operation modes. Thence, there is the unrestricted possibility to reflect the power delivery trend of DVR response during voltage sags. It allows a gradual transition from one power injection level to another with the continuous regulation of two parameters. The properties of the proposed identification tool obtained by the set of three digits can represent the flexible power dispatch.

The rest of the paper is organized as follows. A brief review of the equivalent concept of elliptical trajectory is presented in Section II. In addition, the chosen voltage support scheme and the algorithm of the proposed strategy can also be provided. Mathematical analysis and all necessary vector relationships are presented to demonstrate the strategy for the individual active and reactive power injections in Section III. Section IV verifies the feasibility of the proposed method through selected experimental results. Finally, Section V presents the conclusions of this paper.

II. SYSTEM DESCRIPTION AND MODELING ELLIPTICAL TRANSFORMATION

In order to facilitate all subsequent analysis, this section gives a brief description of the elliptical transformation. Note that there is no consideration for harmonic distortion under voltage sags in this paper.

A. Quantitative Analysis of Elliptical Transformation

Fig.2 shows a typical vector diagram for the elliptical transformation in this paper, as also discussed in [36]. The magnitudes of load voltage and current ($\vec{V}_L$ and $\vec{I}_L$) are constant at rated percentages during all the operating conditions. Based on this principle, the phase difference between the load voltage $\vec{V}_L$ and the instantaneous voltage source $\vec{V}_{sag}$ will happen once a voltage sag occurs. As a result, the injected voltage $\vec{V}_{inj}$ exists a phase shift β with respect to the current reference phasor $\vec{I}_L$. The provision of voltage support will be essential, and it has become a prime target to meet sag-ride through. For better visualization, the graphical representation of the compensation voltage vectors is shown in Fig.3, which is able to describe the individual active and reactive power control. At first, draw one line l_p perpendicular to the horizontal axis, and the given line passes through the top locus of the voltage vector ($\vec{V}_L$) so that the injected active power can remain the specific mapping. Thus, the horizontal injected power P_{inj} is always fixed, and it is aligned with the current vector. There is a new relationship that the top locus of the injected power vector is still located at a particular point of a line segment, which is also a portion of the trajectory (line l_p). At the same time, this injected power is the sum of a constant amount of P_{inj} and arbitrary values of Q_{inj}. Thus, the drawn line l_p can be defined as the equi-active power line. A typical perpendicular injected power component associated with the constant length of P_{inj} holds the same direction of vertical current vector $\vec{I}_L^{\perp}$ and is also proportional to the arbitrary values Q_{inj}. As shown in Fig.3, the vector $\vec{V}_e$ tracing the elliptical trajectory, which begins with point D to any point of the equi-active line l_p as an example at point E, represents one specific compensated voltage. It should be noted that the

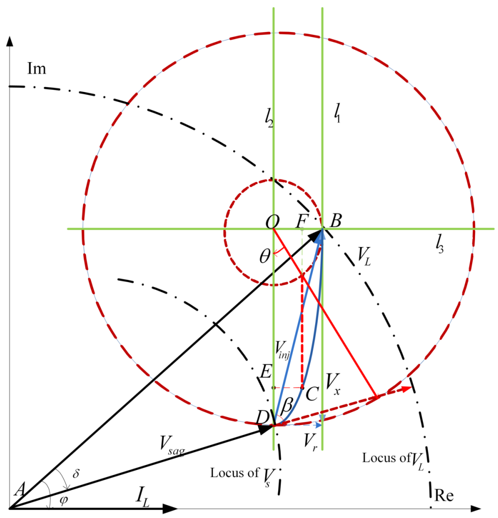

Fig. 2: Graphical representation of elliptical transformation

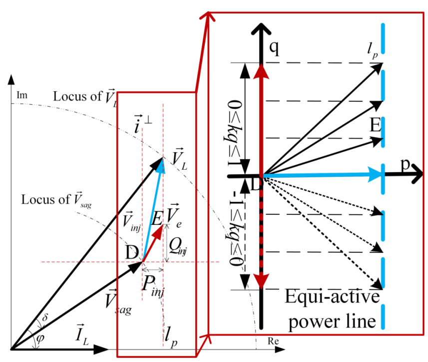

Fig. 3: Phasor diagram describing the proposed equi-active power line

total amount of power injection is the combination of constant P_{inj} and arbitrary values of Q_{inj}.

Again, construct a line l_q parallel to the horizontal axis but at a specific mapping distance equal to the power quantity Q_{inj}. Still, the drawn line l_q can be designed as the equi-reactive power line, as depicted in Fig.4. This line l_q can also be denoted the terminal point locus of injected voltage, and it is the tradeoff between arbitrary amount P_{inj} and constant values Q_{inj}. An adjustable horizontal injected power component associated with the constant value of Q_{inj} maintains the same direction of the current reference, and it is also proportional

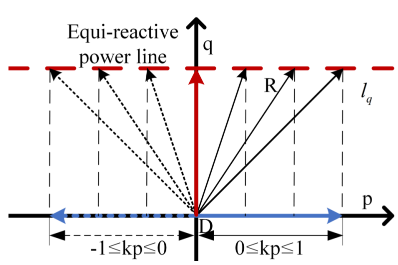

Fig. 4: Phasor diagram describing the proposed equi-reactive power line

to the arbitrary values P_{inj}. As depicted in Fig.4, the vector $\vec{V}_e$, which also begins with point D to any point of the equi-reactive line l_q, for example, at point R, describes the voltage that should be compensated. It should also be seen that the maximum value of output power is the sum of a constant amount of Q_{inj} and an arbitrary amount of P_{inj}.

In sum, by superimposing the vector diagram of the equi-reactive power line l_q onto the equi-active power line l_p, the terminal point locus of the injected voltage can depict particular system condition that satisfies the elliptical trajectory. On the one hand, the arbitrary injected power can be obtained by utilizing the individual controllable active and reactive power components. On the other hand, the strategies based on the power dispatch are realized for two situations as follows:

1) The controllable reactive power: based on the horizontal constant active power, one orthogonal power generator is required to increase the output voltage dramatically. This perpendicular power vector is the key to the control algorithm since the instantaneous injected reactive power can be regulated by selecting an adjustable scalar parameter.
2) The controllable active power: based on a similar analysis, one injected active power generator that satisfies a constant reactive power component can be achieved by choosing a proper scalar parameter. Then, the injected voltage is determined with a combination of both transferred active and reactive powers.

B. New Forms of Adjustable Current Reference Generator

The main purpose of this subsection is to describe the current reference generators by utilizing the elliptical transformation. Since the three double-winding transformers with a neutral of the secondary connected to ungrounded are used to interface the load to the grid in this paper, the zero sequence component is not present. To understand the nature of the compensation strategy, the mathematical models in the stationary reference frame (SRF) can be described ($\vec{v}_\alpha = \vec{v}_\alpha^+ + \vec{v}_\alpha^-$ and $\vec{v}_\beta = \vec{v}_\beta^+ + \vec{v}_\beta^-$) as a function of times.

$$\begin{aligned} \vec{v}_\alpha &= V^+ \sin(\omega t + \varphi_+) + V^- \sin(\omega t - \varphi_-) \\ \vec{v}_\beta &= -V^+ \cos(\omega t + \varphi_+) + V^- \cos(\omega t - \varphi_-) \end{aligned} \tag{1}$$

where $\vec{v}_\alpha^+$, $\vec{v}_\beta^+$ and $\vec{v}_\alpha^-$, $\vec{v}_\beta^-$ are the positive and negative voltage sequences, respectively. V^+ and V^- are their magnitudes. The pair φ_+ and φ_- are the initial phase angles of positive and negative sequence. Then, the computation of output power can be given

$$p = p^+ + p^- \quad q = q^+ + q^- \tag{2}$$

Based on [36], one set of existing current references is defined

$$\vec{i}_p^+ = k^+(k_1 p^+ - k_2 q^+) \qquad \vec{i}_q^+ = k^+(k_3 p^+ - k_4 q^+) \tag{3}$$

$$\vec{i}_p^- = k^-(k_5 p^- - k_6 q^-) \qquad \vec{i}_q^- = k^-(k_7 p^- - k_8 q^-) \tag{4}$$

Obviously, the defined four parameters in (3) can be rewritten as follows:

$$\begin{aligned} k_1 &= -(V^+)^2 - \underbrace{V^+V^- \cos(\theta)}_{\tilde{S}_{2c}} - \underbrace{V^+V^- \sin(\theta)}_{\tilde{S}_{2s}} \\ k_2 &= -V^+V^- \cos(\theta) - V^+V^- \sin(\theta) \\ k_3 &= -V^+V^- \cos(\theta) + V^+V^- \sin(\theta) \\ k_4 &= -(V^+)^2 - V^+V^- \cos(\theta) + V^+V^- \sin(\theta) \end{aligned} \tag{5}$$

where $\theta = 2\omega t + \varphi_+ - \varphi_-$. The $\tilde{S}_{2c}$ and $\tilde{S}_{2s}$ denote the forged power introduced by positive and negative components, respectively. It can be found that the two forged power are orthogonal oscillating terms at twice the fundamental frequency. On the other hand, these oscillating terms also cause power losses and operating current rise, and therefore, this is the main reason why forged power terms ($\tilde{S}_{2c}$ and $\tilde{S}_{2s}$) must disappear. As the first approximation, (5) should be expressed without forged power terms as

$$k_1 = -(V^+)^2 \quad k_2 = 0 \quad k_3 = 0 \quad k_4 = -(V^+)^2 \tag{6}$$

Again, the defined four parameters in (4) will be rewritten as follows:

$$\begin{aligned} k_5 &= -(V^-)^2 - \underbrace{V^+V^- \cos(\theta)}_{\tilde{S}_{2c}} + \underbrace{V^+V^- \sin(\theta)}_{\tilde{S}_{2s}} \\ k_6 &= -V^+V^- \cos(\theta) + V^+V^- \sin(\theta) \\ k_7 &= -V^+V^- \cos(\theta) - V^+V^- \sin(\theta) \\ k_8 &= -(V^-)^2 - V^+V^- \cos(\theta) - V^+V^- \sin(\theta) \end{aligned} \tag{7}$$

Obviously similar to (6), (7) should also be expressed without forged power terms as

$$k_5 = -(V^-)^2 \quad k_6 = 0 \quad k_7 = 0 \quad k_8 = -(V^-)^2 \tag{8}$$

Inserting (6) and (8) into (3)-(4), a new set of reference generators can be also defined as follows:

$$\vec{i}_p^+ = \vec{i}_{\alpha(p+)} + \vec{i}_{\beta(p+)} = \frac{(k_p p - q)(\vec{v}_\alpha^+ + \vec{v}_\beta^+)}{(V^+)^2 + (V^-)^2} \tag{9}$$

$$\vec{i}_q^+ = \vec{i}_{\alpha(q+)} + \vec{i}_{\beta(q+)} = \frac{-(k_q p - q)(-\vec{v}_\alpha^+ + \vec{v}_\beta^+)}{(V^+)^2 + (V^-)^2} \tag{10}$$

$$\vec{i}_p^- = \vec{i}_{\alpha(p-)} + \vec{i}_{\beta(p-)} = \frac{-(p + k_p q)(\vec{v}_\alpha^- + \vec{v}_\beta^-)}{(V^+)^2 + (V^-)^2} \tag{11}$$

$$\vec{i}_q^- = \vec{i}_{\alpha(q-)} + \vec{i}_{\beta(q-)} = \frac{(p - k_q q)(-\vec{v}_\alpha^- + \vec{v}_\beta^-)}{(V^+)^2 + (V^-)^2} \tag{12}$$

where k_p and k_q are the control parameters, respectively. These parameters can take any values from -1 to 1, and also give rise to multiple injection strategies. Next, the selection of control parameters and the complete mathematical analysis will be presented in Section III.

III. Theoretical Approach to the Control Strategy

The best way to accomplish the proposed reference generators is a smart selection of k_p and k_q. Obviously, there are infinite combinations with these double parameters (k_p and k_q) in (9)-(12).

A. Targets for the Positive and Negative Sequence Currents

To distinguish clearly between the symbol k_p and k_q, the parameter utilized to control the active and reactive power separately in the following is defined as k_{pq}. The reference injected power p^* and q^* can be displayed in the pq space vector plane. In such a plane, the injected active and reactive powers coincide with the p axis [real axis (Re)] and q axis [imaginary axis (Im)], respectively. Hence, the reference injected power, named apparent power s^*, can be derived by adding (2)

$$s^* = k_{pq}(p_m^* + jq_m^*) \tag{13}$$

where $j = \sqrt{-1}$, m = a,b, or c. Therefore, there are infinite combinations with the changeable parameter of k_{pq} in (13). It can also be seen that the linear controllability benefiting from previous individual power control schemes can not exist. Therefore, two joint strategies are proposed to simplify (13) by utilizing the reference active and reactive powers.

1) Joint strategy with the positive-sequence control

By setting $k_p = k_q = k_{pq}$, reference apparent power is simplified and rewritten as follows:

$$s^* = (k_{pq}p_m^* + jq_m^*) \tag{14}$$

As shown in Fig.5a, when k_p changes from 0 to 1, the length of apparent power vector changes within the first quadrant of a Cartesian coordinate. The apparent power trajectory is directed to the sliding line (denoted by the parameter k_p). It slides along the sliding line toward the origin, which determines the boundaries of the existing regions. On the other hand, apparent power also varies with the change if $-1 \leq k_p \leq 0$, and it is entered the second quadrant of a Cartesian coordinate. The parameter k_p divides the apparent power into two regions. The sliding action occurs on the areas between the blue line and the p axis.

2) Joint strategy with the negative-sequence control

By setting $k_p = -k_q = k_{pq}$, reference apparent power is, again, rewritten as follows

$$s^* = (p_m^* + jk_{pq}q_m^*) \tag{15}$$

Illustrative plots are drawn in Fig.5b. It can be seen from (15) that this joint strategy also splits the apparent power into two areas. The existing region is determined by two red lines and the p axis. To observe the controllability, a simple analysis reveals that merging strategies 1) and 2) can be put together, and the proposed reference generators are also normalized as follows:

$$\vec{i}_\alpha^{+*} = \vec{i}_{\alpha(p+)}^* + \vec{i}_{\alpha(q+)}^* = \frac{(k_{pq}p^* - q^*)(\vec{v}_\alpha^+ - \vec{v}_\beta^+)}{(V^+)^2 + (V^-)^2} \tag{16}$$

$$\vec{i}_\alpha^{-*} = \vec{i}_{\alpha(p-)}^* + \vec{i}_{\alpha(q-)}^* = \frac{-(p^* - k_{pq}q^*)(\vec{v}_\alpha^- - \vec{v}_\beta^-)}{(V^+)^2 + (V^-)^2} \tag{17}$$

$$\vec{i}_\beta^{+*} = \vec{i}_{\beta(p+)}^* + \vec{i}_{\beta(q+)}^* = \frac{(k_{pq}p^* - q^*)(\vec{v}_\alpha^+ + \vec{v}_\beta^+)}{(V^+)^2 + (V^-)^2} \tag{18}$$

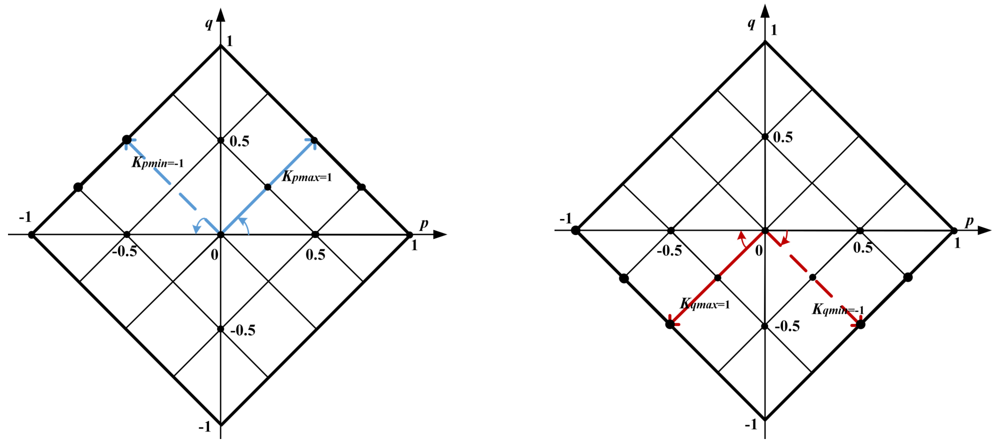

(a) (b)

Fig. 5: Apparent power trajectories in pq space system (a) where $-1<k_p = k_q=k_{pq}<1$ and (b) where $-1<k_p=-k_q=k_{pq} < 1$

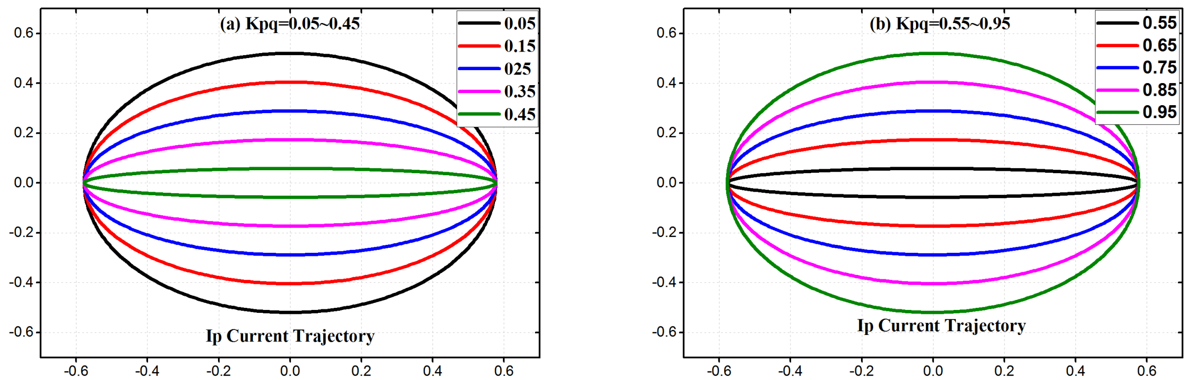

(a) (b)

Fig. 6: I_p current trajectories with k_{pq} in $\alpha\beta$ system (a) where $0<k_p=k_q=k_{pq}<0.5$ and (b) where $0.5<k_p=k_q=k_{pq} < 1$

$$\vec{i}_{\beta}^{-*} = \vec{i}^*_{\beta(p-)} + \vec{i}^*_{\beta(q-)} = \frac{-(p^* - k_{pq}q^*)(\vec{v}_{\alpha}^- + \vec{v}_{\beta}^-)}{(V^+)^2 + (V^-)^2} \quad (19)$$

The different active and reactive power dispatches can be achieved by selecting k_{pq} (k_p or k_q) inside the range of $-1 < k_{pq} < 1$. From (16)-(19), the output currents depend on the control parameter, voltage characteristics, and the references active and reactive powers. For instance, the resulting p-component current can be regulated by k_{pq}, and the graphical diagram is plotted under the given phase angle $\varphi = \varphi_+ - \varphi_-$ (for example, 30°). I_p current trajectories shown in Fig.6a are obtained by setting k_{pq} from 0 to 0.5, and the results are also demonstrated in Fig.6b from 0.5 to 1. As shown in Fig.7, I_p current trajectories can be obtained when k_{pq} is adjusted from -1 to 0. It can also be seen that the length of the p-component current reference can decrease to the minimum value when k_{pq} moves towards -0.5.

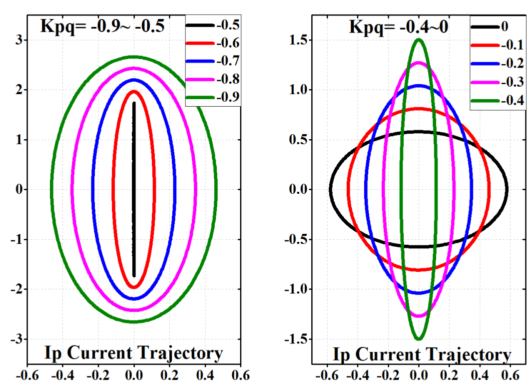

Fig. 7: I_p current trajectories with k_{pq} where $-1 < k_p = -k_q = k_{pq} < 0$ in $\alpha\beta$ system

B. Modeling and Analysis of Identification Design

The main aspects of the two joint strategies are tabulated in Table I. Strategy 1) can only describe one changeable requirement of the active power, whereas strategy 2) allows more flexible controllability of the reactive power. In summary, the adaptive controllability of individual power control is preserved in the presented joint approaches. It enables the DVR system to be optimized under voltage sags and makes it flexible to satisfy the load requirements. During voltage sags, the apparent power rotates around the geometric center (i.e., point 0 in Fig.5) depending on which the adjustable parameters k_p or k_q have been chosen. The main axis occupies a leading

This article has been accepted for publication in a future issue of this journal, but has not been fully edited. Content may change prior to final publication. Citation information: DOI 10.1109/JESTPE.2020.3047151, IEEE Journal of Emerging and Selected Topics in Power Electronics

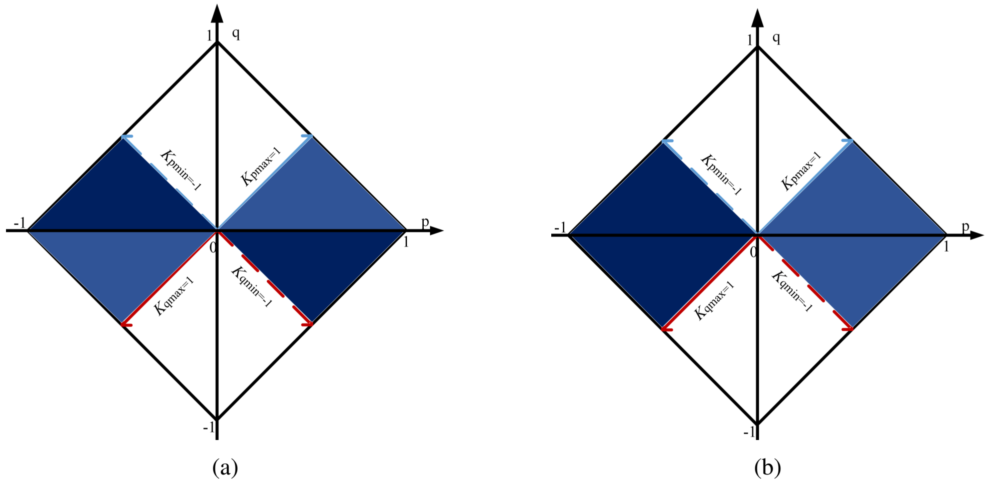

Fig. 8: Graphic representation of (a) existing regions of the active power control, and (b) existing regions of the reactive power control

TABLE I: Controllability of Joint Strategies

Description	$[0, 1]$	$[-1, 0]$
active power parameter	100	111
reactive power parameter	001	010

position compared to the abscissa axis. This angle is used as the mark that identifies the compensation strategies. Hence, the representative variables of the terminal point locus have been codified. This digital code indicated in the last two columns of Table I allows a fast procedure to identify the type of chosen parameter. The first digit represents the orientation state based on the horizontal axis (joint strategy with active power control = '1'; joint strategy with reactive power control = '0'). The second and third digits are associated with the presence of compensation strategies ($k_p = k_q = k_{pq} \in [0, 1]$ = '00'; $k_p = k_q = k_{pq} \in [-1, 0]$ = '11'; $k_p = -k_q = k_{pq} \in [0, 1]$ = '01'; $k_p = -k_q = k_{pq} \in [-1, 0]$ = '10').

Considering the distribution areas of the parameter (k_{pq}), the light blue triangles as depicted in Fig.8a, corresponding to the joint strategy with active power control, describe the portion of $[0, 1]$, in which this existing region is controlled with the code selection of "00". However, the dark counterpart represents the situation of $[-1, 0]$, in which the proposed region is controlled with the code selection of "11". At the same time, the representative variables with reactive power control have also been codified similarly in Fig.8b. The light blue triangles provide information in which the given region can be guaranteed using code "01" if $k_p = -k_q = k_{pq}$ is set to $[0, 1]$. Also, it can be observed that the dark blue triangles can be codified by utilizing "10" when $k_p = -k_q = k_{pq}$ is regulated within the range of $[-1, 0]$. Therefore, the flexible identification tool created by the digit codes is obtained by selecting two parameters (k_p and k_q).

As Fig.9a shows, the contour color map is presented within the first quadrant of the p-q axis system, where the more affected areas are marked between the dotted line in blue and the p axis, and the areas which are subject to the reactive power control are marked between the red line and the reference abscissa. The blue line and the red line denote the maximum and minimum boundaries of the two control parameters, respectively. In this figure, the smaller the parameter k_q, the larger the controllable reactive power. The given variable Q (or -Q) denotes the controllable reactive power which is decided by the parameter k_q inside the ranges from -1 to 0. At the same time, the adjustable active power gradually decreases as the value of the parameter k_p decreases. In Fig.9a, three parameters k_{p1}, k_{p2} and k_{p3} denote the indices of the flexible ranges which are less than 1, respectively. The horizontal solid line in green represents the adjustable active power. In this way, the three green solid dots in the p-axis represent the main characteristic of the adjustable active power. Their locations determine the actual amount of active power. In addition, the vertical solid line in green represents the reactive power decided by the parameter k_q.

To account for variation in the power requirements during voltage sags, the knee points of the adjustable active power are randomly located by varying p-axis values according to preset parameter distributions (e.g., k_{p1}, k_{p2} and k_{p3}). The number of knee points corresponding to preset parameter distributions is generated within the value range of the parameter k_p. In reality, these knee points accurately describe the gradual transition from one adjustable active power level to another. The joint regions including two neighboring active power ranges can be easily identified. Also, these preset parameter distributions approximate the adjustable trend of the active power dispatch embedded in the existing control strategy. In a specific application, one single knee point can be selected according to an actual control strategy if the relationship of $k_p = -k_q = k_{pq}$ is satisfied. In this case, the flexible power dispatch with the controllable reactive power and the adjustable active power can be decided by using the digital codes of '001'.

Compared to Fig.9a, it can be seen from Fig.9b that a crisp green line at the joint region including two neighboring active power ranges is obtained in this case once the

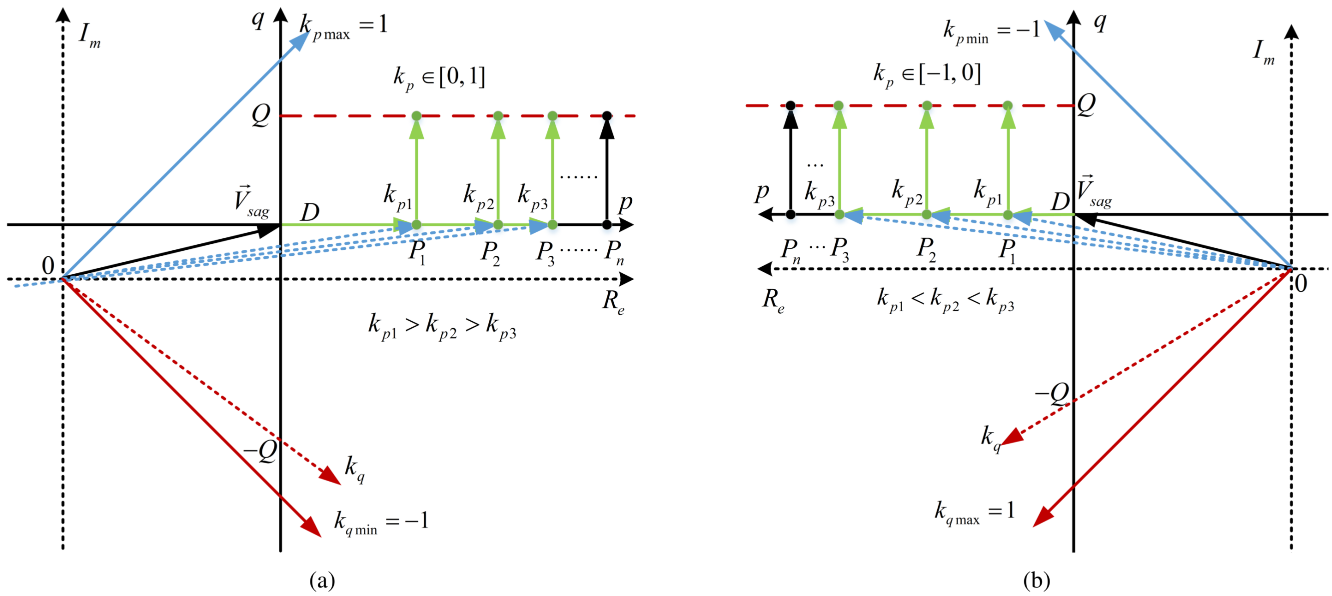

Fig. 9: Graphic representation of (a) existing regions of the reactive power control when $k_p \in [0,\ 1]$ and $k_q \in [-1,\ 0]$, and (b) existing regions of the reactive power control when $k_p \in [-1,\ 0]$ and $k_q \in [0,\ 1]$

corresponding parameter distributions are selected. Given the flexible selection of the knee points, two control parameters k_p and k_q can be adjusted according to specific cases in practical applications. In Fig.9b, one single knee point can also be chosen according to an actual control strategy if the the relationship of $k_p = -k_q = k_{pq} \in [-1,\ 0]$ is satisfied. Then, the flexible power dispatch with the controllable reactive power and the adjustable active power can be decided by using the digital codes of ’010’.

Also, the same reasoning holds for another strategy known as the flexible power dispatch with the controllable active power and the adjustable reactive power. The whole digital codes are recorded as ”100’ once the condition that the $k_p = k_q$ satisfies the rule of $k_{pq} \in [0,\ 1]$. Furthermore, when the two control parameters perform the rule of $k_p = k_q = k_{pq} \in [-1,\ 0]$, one set of digital codes can be noted as ’111’. Then, the corresponding power dispatch can also be designed similar to Fig.9a-Fig.9b.

C. Proposed Control Scheme

Also, further discussion to illustrate the selection of the control parameters is required. Fig.10 depicts the simplified diagram of the control proposal. Then, it is clear evidence that the reference injected voltages can be increased to a safe predefined value. In the first three blocks, the voltage at the point of common coupling (PCC) is measured and computed based on the elliptical trajectory. Then, the next step is responsible for estimating the voltage vectors using a sequence extractor. The core of the compensation algorithm is the Mux block, and two reference blocks can calculate the new current references using the offline selection of k_{pq} (or k_p, k_q). Next, the current loop in the last block is proposed to reduce the error in a steady state. Afterwards, the reference reactive power can also be approximately obtained by multiplying current

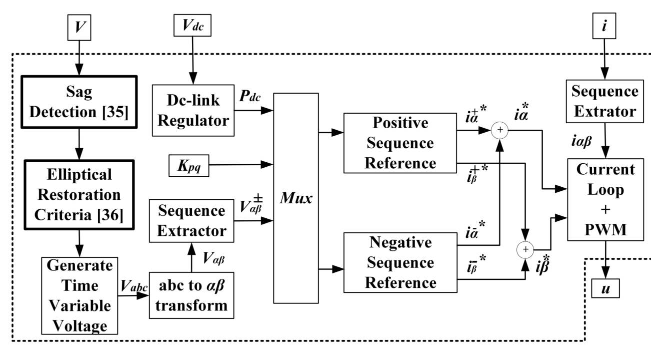

Fig. 10: Complete block diagram of the proposed algorithm

reference by positive voltage, i.e. $q^* = I_q^*((\vec{v}_\alpha^+)^2 + (\vec{v}_\beta^+)^2)^{0.5}$. At the same time, the reference active power satisfies the condition of $p^* = P_{dc}$, as shown in Fig.11.

Different types of voltage sag can be programmed: (1) before 0.1s, PCC voltages are steady-state condition; (2) at time t = 0.1s, a voltage sag of 0.5 p.u. with a phase jump δ of $+25°$ occurs (Type A sag [37]). Afterwards, from t = 0.1s to 0.4s, the proposed active and reactive power dispatches start by means of (16)-(19). Finally, the control algorithm is disabled when the voltage sags are clear at time t = 0.4s. Fig.12 shows this representative case of voltage sag.

The first way, named as Case A, is designed for the mentioned voltage condition. Also, the same reasoning, again, holds for another scheme known as Case B and Case C. In particular, the unique requirements of this strategy for different applications can be shown in the first two columns of Table II. At the same time, the horizontal scale of all figures is marked as the 40 ms/div, which is utilized to display the time range in each experimental result.

This article has been accepted for publication in a future issue of this journal, but has not been fully edited. Content may change prior to final publication. Citation information: DOI 10.1109/JESTPE.2020.3047151, IEEE Journal of Emerging and Selected Topics in Power Electronics

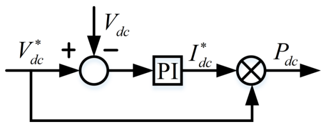

Fig. 11: The dc-link voltage control

TABLE II: The Measured Active Power (Watts) and Reactive Power (Vars)

Schemes	Adjust parameter	$\bar{p}^+ + \bar{p}^-$	$\bar{q}^+ + \bar{q}^-$
Case A	$k_p = 0.5 \rightarrow 0.7 \rightarrow 0.9$ $k_q = 0.5 \rightarrow 0.5 \rightarrow 0.5$	165 → 210 → 240	150
Case B	$k_p = -0.6 \rightarrow -0.6 \rightarrow -0.6$ $k_q = 0.9 \rightarrow 0.6 \rightarrow 0.3$	185	300 → 200 → 90
Case C	$k_p = -0.9 \rightarrow -0.6 \rightarrow -0.3$ $k_q = -0.6 \rightarrow -0.6 \rightarrow -0.6$	250 → 190 → 90	190

TABLE III: System Parameters for DVR Setup

DVR (exclude injected transformer)		Injected Transformer of DVR	
Parameter	Value	Parameter	Value
Grid Frequency	50Hz	Power	4.5 kVA
Filter Inductance	1.4 mH	Primary Voltage	310V
Filter Capacitance	15 μF	Secondary Voltage	310V
Vdc Voltage	180V	Magnetization Resistance	200 p.u.
load power	3 kW 0.83PF lag	Magnetization Inductance	200 p.u.

IV. Experimental Analysis

This section validates the theoretical contributions of this paper by experimental results. A dSPACE DS1202 hardware has been utilized as the control platform. The sag source has been emulated by using a Chroma programmable ac source 61611. A Chroma programmable ac electronic load 63804 is served as the three-phase sensitive load, and one Danfoss FC 302 converters are used as a three-phase IGBT bridge. The details of the power configuration are shown in Fig.13. Table III provides the main parameters of the experimental test setup.

A. Tests of the Joint Strategies During Voltage Sag

A set of experiments is conducted to evaluate the proposed reference generators. Observe that the measured reactive power is nearly 150Var shown in Fig.14a, which tracks the parameter $k_q = 0.5$. However, the measured active power is almost 165W during the period t = 0.1s to 0.2s. Then, this value is increased up to 210W, and the final amount of the measured value is equal to 240W, given in Fig.14a, because the control

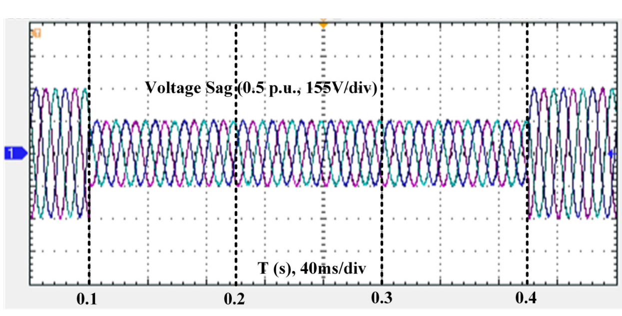

Fig. 12: One representative case of voltage sag with 0.5 p.u.

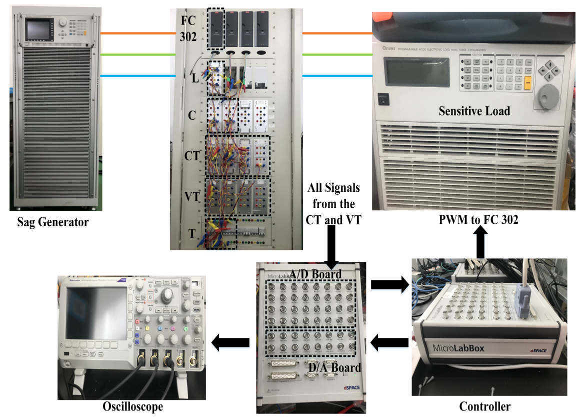

Fig. 13: Details of the power circuit used in the experiment.

parameter is continuously shifted ($k_p = 0.5 \rightarrow 0.7 \rightarrow 0.9$). The injected voltage curves are shown in Fig.14b. The volage sag magnitude and the load voltage magnitude are also shown in Fig.14c. The dc-link voltage is shown in Fig. 14d. It can be seen that the control scheme with the controllable active power and constant reactive power can be implemented by selecting two parameters in Case A. Thus, the first digit of the identification tool is '1'. In addition, the last two digits of the identification tool satisfy the digital codes of '00' since the two parameters perform the rule of $k_p = k_q = k_{pq} \in [0,\ 1]$ inside the time range from 0.1 s to 0.2 s. Then, this proposed identification marks can decide to the flexible power dispatch with the controllable active power and constant reactive power by using the digital codes of '100'.

Dynamic waveforms are shown in Fig.15, in comparison with the results depicted in Fig.14. Note that the measured reactive power is increased from 0 to a maximum value of 300Var. Then, this value is reduced to 200Var, and the final amount of the measured value is equal to 90Var shown at the foot curve of Fig.15a when the control parameter is continuously shifted ($k_q = 0.9 \rightarrow 0.6 \rightarrow 0.3$). The measured active power is increased from 0 to a rough value of 185W as depicted at the peak curve in Fig15a, where the control parameter is $k_p = -0.6$. The load voltage in Fig.15b can be compensated adequately and also kept at an acceptable state (1.0 p.u.). It can be observed that the load voltage is restored to the nominal value with the constant active power injection and adjustable value of the reactive power injection. The first digit of the identification tool is marked as '0' when the two parameters are chosen in Case B. The last two numbers of the identification tool are given as '10' since the Case B within the time range between 0.2 s and 0.3 s satisfies the rule of $k_p = -k_q = k_{pq} \in [-1,\ 0]$. As a result, one set of digital codes can be noted as '010' in order to achieve the presented control scheme.

Fig.16 depicts the experimental results of the proposed Case C. It is interesting to note that the maximum value of the measured active power is 250W, then this value is decreased to 190W, and the final amount of this active power is equal to 90W, while the measured value of the reactive power is almost 190Var, as displayed in Fig.16a. The load voltages are

This article has been accepted for publication in a future issue of this journal, but has not been fully edited. Content may change prior to final publication. Citation information: DOI 10.1109/JESTPE.2020.3047151, IEEE Journal of Emerging and Selected Topics in Power Electronics

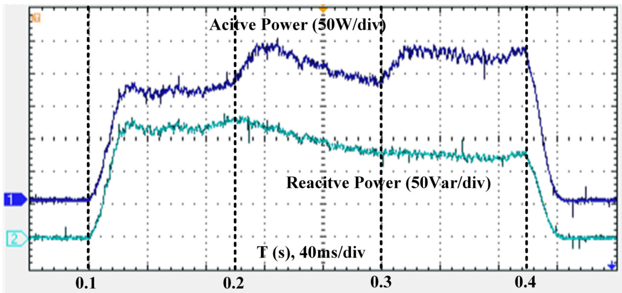

(a)

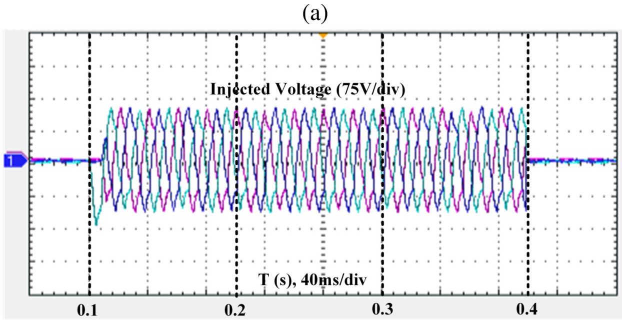

(b)

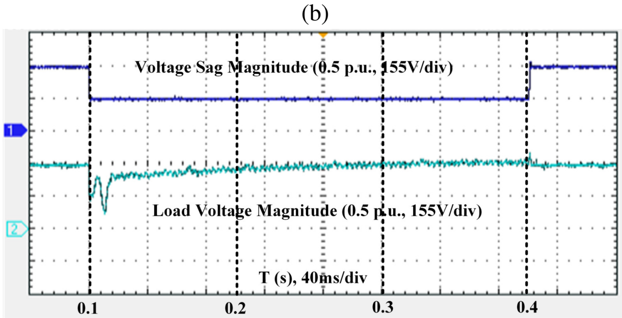

(c)

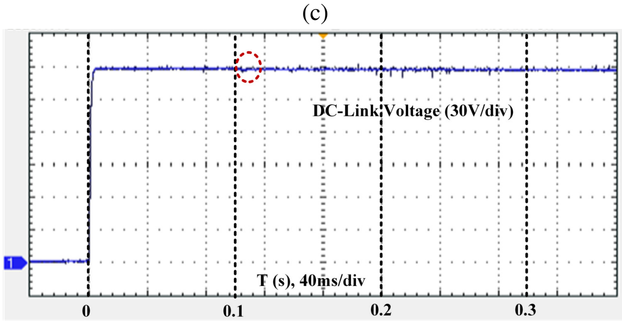

(d)

Fig. 14: Experimental results for Case A.

shown in Fig.16b. Fig.16a reveals that the proposed control scheme with the flexible active power injection and constant reactive power injection is obtained during Case C. Thus, the first number of the identification tool is recorded as '1'. Because of the condition that the $k_p = k_q$ satisfies the rule of $k_{pq} \in [-1,\ 0]$ inside the time range from 0.2 s to 0.3 s, the last two digits of the identification tool meets the digital codes of '11'. Then, the whole digits of the identification tool are recorded as '111'.

To summarize, Table II includes the main results of the given three strategies. Besides, the three control schemes demonstrate the smooth transition during changes in the control parameters during voltage sags and the elimination of active and reactive power oscillations.

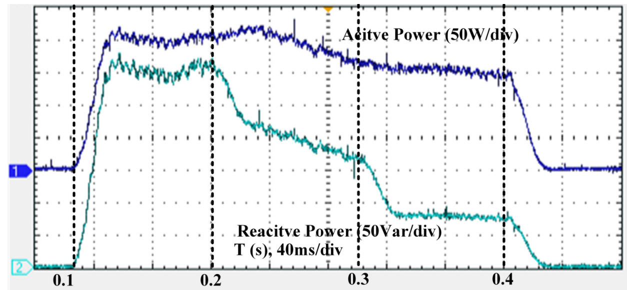

(a)

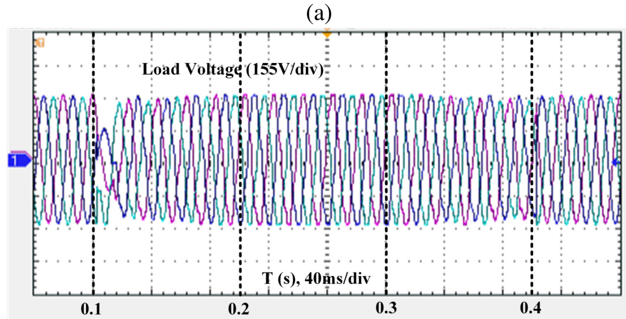

(b)

Fig. 15: Experimental results for Case B.

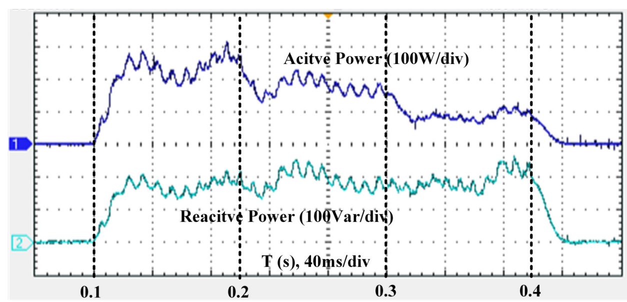

(a)

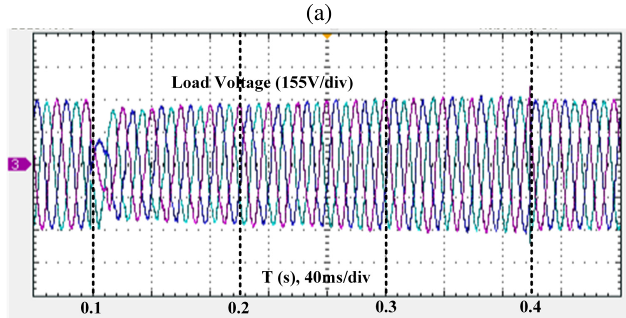

(b)

Fig. 16: Experimental results for Case C.

B. Performance With Different Types of Voltage Sag

A complete set of experimental tests has been carried out to reveal the feasibility of the control scheme under different voltage sags. In this situation, two different voltage sags and one type of voltage swell have been programmed to evaluate the behavior of the system. Therefore, a single-phase voltage

This article has been accepted for publication in a future issue of this journal, but has not been fully edited. Content may change prior to final publication. Citation information: DOI 10.1109/JESTPE.2020.3047151, IEEE Journal of Emerging and Selected Topics in Power Electronics

sag (a-phase) of 0.4 p.u. is experienced in Test 1 (Type B sag [37]), in which the control parameter is modified ceaselessly ($k_q = -0.2 \rightarrow -0.5 \rightarrow -0.8$) in view of the control parameter ($k_p = 0.5$). Test 2 (Type C sag [37]) suffers a two-phase voltage sag (b- and c-phase) of 0.8 p.u., in which the control parameter is continuously changed ($k_p = 0.2 \rightarrow 0.5 \rightarrow 0.8$) by considering the control parameter ($k_q = 0.5$). Three phases voltage swell of 1.1 p.u., marked as the Test 3, is also occurs when the control parameters are changed during the Case A. Then, this two types of voltage sags and one type of voltage swell are shown in Fig.17.

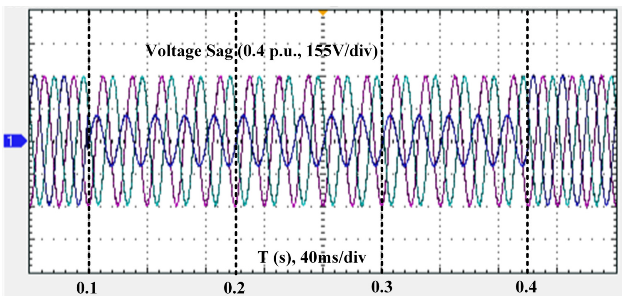

(a)

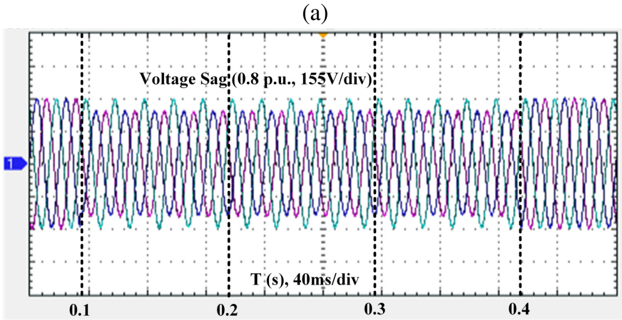

(b)

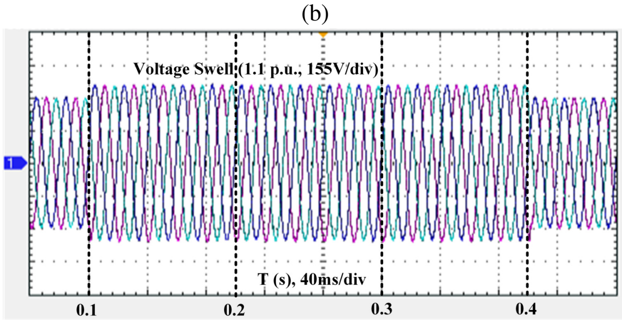

(c)

Fig. 17: Two representative cases of voltage sag with 0.4 p.u. and 0.8 p.u.; one representative case of voltage swell with 1.1 p.u.

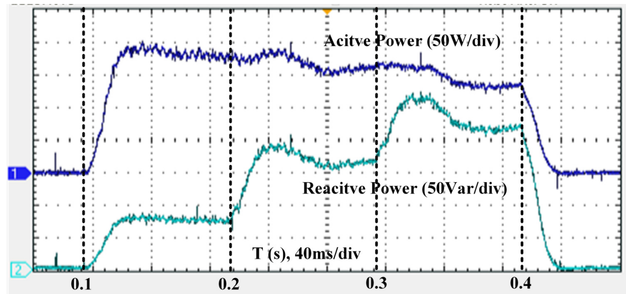

(a)

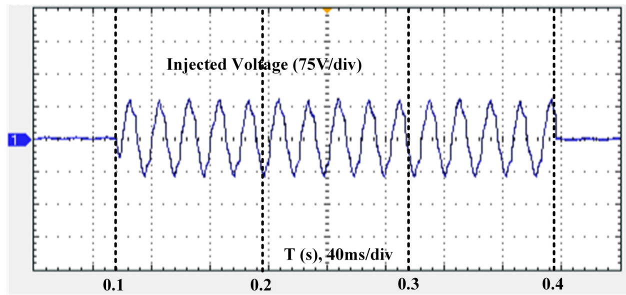

(b)

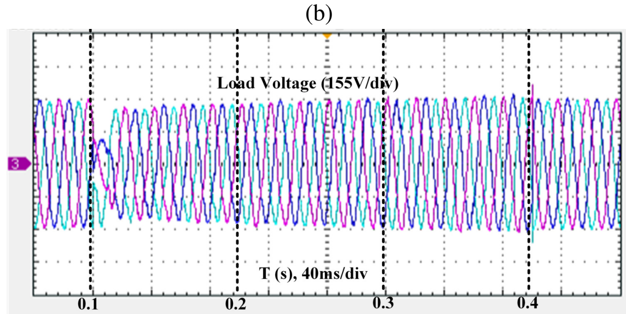

(c)

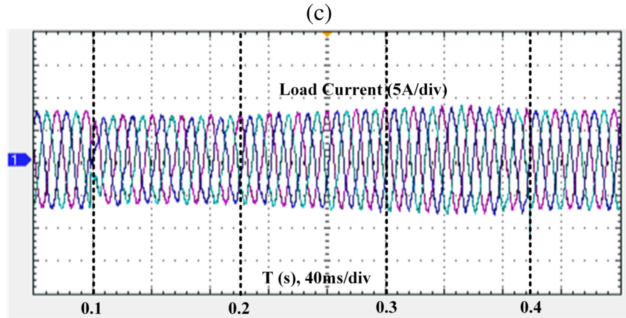

(d)

Fig. 18: Experimental results for Test 1.

Fig.18 shows the experimental result when the PCC voltage is perturbed by Test 1. Note that the measured active power is close to 175W, shown at the high level of Fig.18a. The measured value of the injected reactive power is 80Var at the bottom of the low level in Fig.18a. And then, this value is increased up to 180Var in the middle of the low level in Fig.18a. The maximum value of the measured reactive power is equal to 245Var at the top of the low level in Fig.18a. The injected voltage in Fig.18b can compensate for the load voltage effectively. Fig.18c shows the load voltages and the load currents are shown in Fig.18d. It is important to note that the presented control scheme with the constant active power injection and adjustable reactive power injection is obtained by selecting the condition of $k_p = -k_q = k_{pq} \in [0,\ 1]$. Therefore, a new set of digital codes (i.e., '001') can be used to determine the identification tool inside the time range from 0.2 s to 0.3 s.

Fig.19 depicts the experimental waveform when the PCC voltage is perturbed by Test 2. Observe that the measured reactive power has been an increase of roughly 165Var represented at the lower curve of Fig.19a. Moreover, the measured value of the injected active power is 55W at the bottom of the upper

This article has been accepted for publication in a future issue of this journal, but has not been fully edited. Content may change prior to final publication. Citation information: DOI 10.1109/JESTPE.2020.3047151, IEEE Journal of Emerging and Selected Topics in Power Electronics

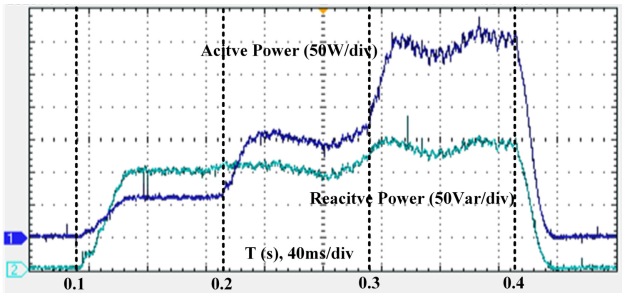

(a)

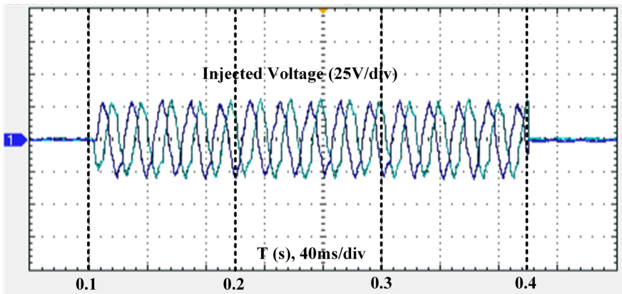

(b)

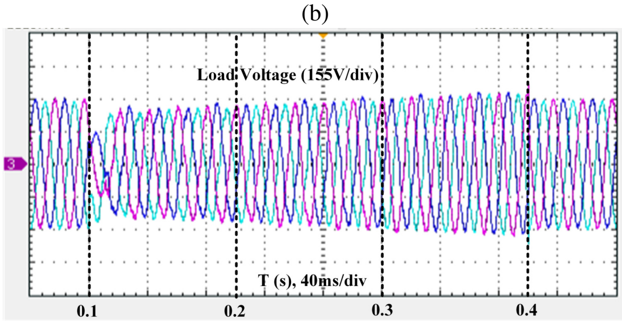

(c)

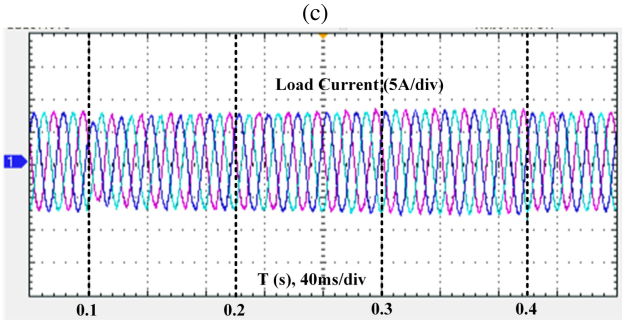

(d)

Fig. 19: Experimental results for Test 2.

curve in Fig.19a, then this value is increased up to 150W at the middle of the high curve in Fig.19a, and the maximum amount of the measured active power is equal to 290W at the top of the high curve in Fig.19a. Again, the injected voltage in Fig.19b can also be given based on the elliptical trajectory compensation. Fig.19c shows the load voltages and the load currents are shown in Fig.19d. Also, the flexible active power injection and constant reactive power injection can be fulfilled when the PCC voltage is perturbed by Test 2. Thus, the three digital numbers of the identification tool can be marked as '100' since the condition of $k_p = k_q$ satisfies the rule of $k_{pq} \in [0,\ 1]$.

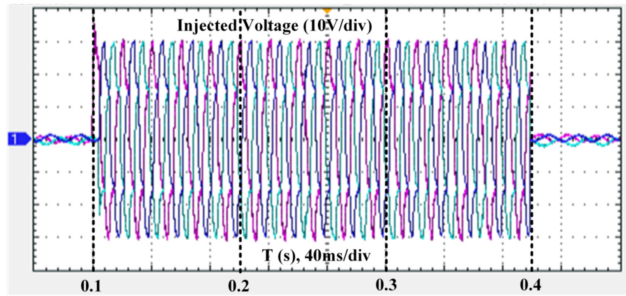

(a)

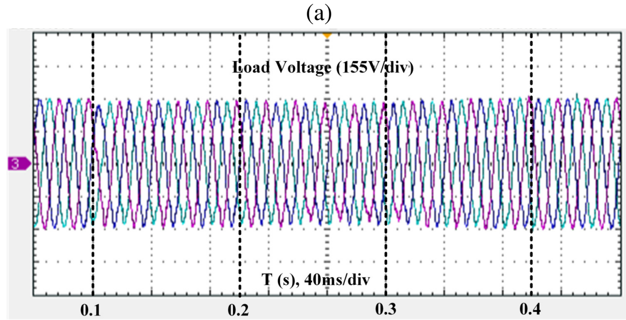

(b)

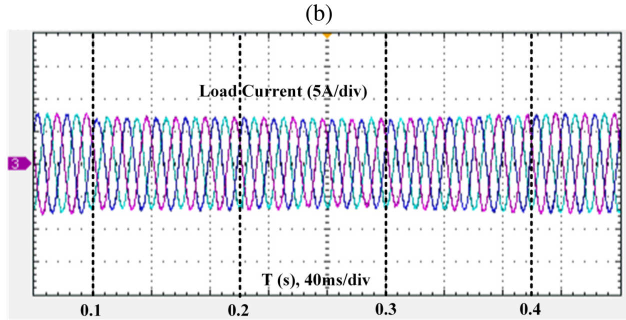

(c)

Fig. 20: Experimental results for Test 3.

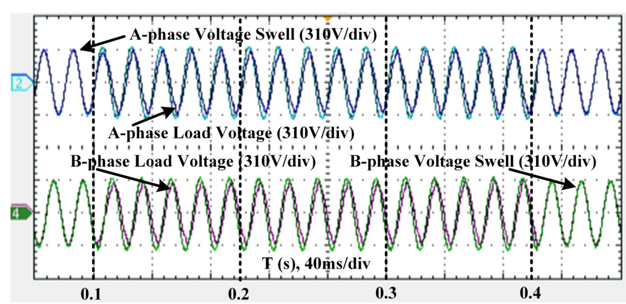

(a)

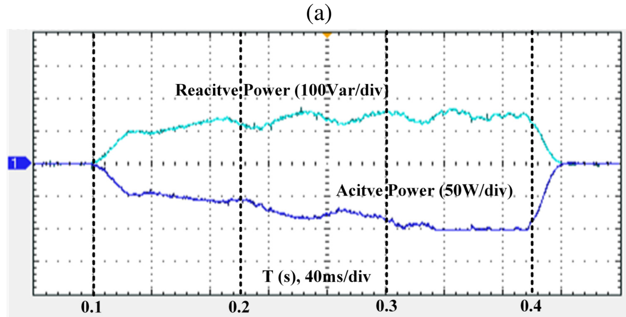

(b)

Fig. 21: Experimental results for Test 3.

TABLE IV: Operating States During the Different Sags

State	Test 1	Test 2	Test 3
Sag Depth (p.u.)	0.4	0.8	1.1 (Swell)
$\bar{q}^+ + \bar{q}^-$ (Var)	80 → 180 → 245	165	120
$\bar{p}^+ + \bar{p}^-$ (W)	175	55 → 150 → 290	-50 → -75 → -100

TABLE V: Comparison with previous strategies of dynamic response

Dynamic Response	Strategy					Proposal
	[28]	[29]	[30]	[31]	[32]	
Time (ms)	13	10	20	25	12	16

Fig.20 depicts the experimental waveform when the PCC voltage is perturbed by Test 3. Note that the injected voltage curves are shown in Fig.20a. And then, the load voltage and the load current are also given in Fig.20b-20c. In addition, the voltage phase plots (a-phase an b-phase) between the voltage swell and the load voltage is shown in Fig.21a. Observe that the measured reactive power is close to 120Var, shown at the high level of Fig.21b. Moreover, the measured value of the injected active power is -50W at the top of the lower curve in Fig.21b, then this value is decreased to -75W at the middle of lower curve in Fig.21b, and the minimum amount of the measured active power is equal to -100W at the bottom of the lower curve in Fig.21b.

In sum, these experimental results are validated automatically by the proposed scheme. Table IV presents the significant characteristics of the previous strategies.

C. Discussion on the Benefits of the Identification Tool

Table II and Table IV display a comparison of different power injections when implementing the proposed control schemes. The control strategies considered in this paper can be identified by employing two adjustable parameters according to the mathematical relationship between the horizontal injection power and the vertical injection power in the elliptical trajectory. At the same time, the presented control strategies give priority to the controllable power injection, which matches correctly with the constant power injection. The main advantage of the presented identification tool is to display the digital codes and thus facilitate the multiple available selections of the active and reactive power dispatch during different voltage sags.

However, it is important to see that the load voltage in Fig.15b and Fig.16b are slightly distorted when the voltage sag occurs. IEEE-1159 defines voltage sag as a RMS voltage decrease to between 0.1 p.u. and 0.9 p.u. for duration from 0.5 cycle to 1 minute [38]. The survey of power quality presents that voltage sags with $40\%-50\%$ of the nominal value and with the duration from 5 to 30 cycles occurred in about 92% of all power system events [39]. This transient response is within one cycle (e.g., 16ms). There are three reasons that lead to the slight undershoot in two of three voltage phases. The first reason is the abrupt parameter change at $t = 0.1s$. The second reason is the dead-time influence of the Danfoss FC 302 converter utilized in the experimental test. The last reason is one fixed delay when the sequence extractors are adopted to detect the voltage sequence components. Table V displays a comparison of different dynamic response when implementing the proposed control strategy and conventional control strategies [28]–[32]. By proper changing of two control parameters in (9)-(12), the appropriate strategy is easy to be decided once the equivalent impedance of sag source and the sag depth at the PCC are found.

Based on the aforementioned set of experiments, the main advantage of this identification tool is fully flexible operation that allows to define the behavior of the DVR in different grid scenarios. On the one hand, if the considered scenario deals with a voltage sag in a stiff grid, the adjustable reactive power injection will produce little influence on the voltage at the PCC. Thus, the factor that plays a vital role is in the selection of flexible active power delivery. On the other hand, the process of putting active and reactive power injection together is required to improve the voltage profile at the PCC when the sag-source with high resistive behavior is considered. Under this consideration, the best solution seems to be to raise the voltage in all phases when the parameter k_p being monotonically changing occurs. Opposite to the mentioned scenario, the choice of adjustable reactive power injection will have a significant effect on the voltage characterization at the PCC if the sag-source is mainly inductive and weak. In this sense, the best solution can be obtained with the smart voltage support service when the parameter k_q being monotonically tuning occurs.

In other words, the decision on which the suitable power injection is the best for the presented scenarios can be achieved by selecting the first digital code of the identification tool. In the following, four scenarios will be investigated to discuss the possible power dispatches. The first scenario consists of obtaining the maximum active power delivery. When the constant value of k_q is selected, the maximum active power dispatch can be achieved once the parameter k_p being monotonically increasing occurs. In this case, the corresponding digital codes of the identification tool is noted as ’100’. The second scenario is made up of obtaining the minimum reactive power delivery. By choosing the constant parameter of k_p, the minimum reactive power delivery can be obtained once the parameter k_q being monotonically decreasing occurs. The corresponding digital codes of the identification tool is remarked as ’010’. The third scenario is to be capable of the minimum active power delivery. When setting the constant value of k_q, the minimum active power delivery can be finished once the parameter k_p being monotonically increasing occurs. The corresponding digital codes of the identification tool is recorded as ’111’. The fourth scenario deals with the maximum reactive power delivery. By selecting the constant value of k_p, the maximum reactive power delivery can be obtained once the parameter k_q being monotonically decreasing occurs. The corresponding digital codes of the identification tool is written as ’001’.

Thus, the main contribution of the identification tool is a straightforward manner using the triplet of the digital codes to obtain different power deliveries during voltage sags. The important application is to prioritize the controllable power

TABLE VI: Comparison with Previous Strategies

Strategy	Studied Mechanism	Active Power Control	Reactive Power Control	Experimental Power Quality Index		
				Zero P Oscillation	Zero Q Oscillation	Smooth Transition
[28]	-	Yes	-	Yes	-	-
[29]	-	-	Yes	-	Yes	-
[30]	-	Yes	Yes	Yes	No	No
[31]	-	Yes	Yes	Yes	No	Only P
[32]	Maximum Current Limit	Yes	Yes	Yes	Yes	No
[33]	Maximum Voltage Limit	Yes	Yes	Yes	Yes	No
[34]	Maximum Power Limit	Yes	Yes	Yes	Yes	No
Proposal	Triple of Digital Codes	Yes	Yes	Yes	Yes	Yes

-: No Application

injection with this triplet of digital codes to fully explore the capacities of the power dispatch, which corroborates that the presented control strategy is able to comply with the load voltage requirements even in different grid scenarios.

D. Comparison With the Conventional Strategy

In the literature, most studies discuss the behavior of eliminating active and reactive power oscillations in different scenarios to increase the immunity against voltage sags. Thus, the mentioned conventional strategies in [28]–[34] have been selected to define the current references (i.e., $\vec{i}_\alpha^* = \vec{i}_\alpha^{+*} + \vec{i}_\alpha^{-*}$ and $\vec{i}_\beta^* = \vec{i}_\beta^{+*} + \vec{i}_\beta^{-*}$), where the different forms of control parameter designed in (16)-(19) can be analyzed to obtain the control objectives.

Table VI provides a comparison between the representative strategies and the mentioned strategy in this paper. Obviously, the considered control strategies in the second column of Table VI incorporate the different mechanisms. Furthermore, the first control strategy in [28] provides a remarkable feature of active power injection that permits to mitigate the active power oscillation. Opposite to the first control strategy, the second one in [29] provides a remarkable feature of reactive power injection that permits to mitigate the reactive power oscillation. The third control strategy in [30] provides a remarkable feature of active and reactive power injection that permits to maximize power delivery capability, while the oscillation terms of the active and reactive power cannot be avoided. The fourth control strategy in [31] provides a remarkable feature of active and reactive power injection that permits to mitigate the active power oscillation. The fifth control strategy in [32] provides a remarkable feature of active and reactive power control that permits to obtain the zero oscillation of active and reactive power injection, while the maximum current limit can exceed the rated current (i.e., I_{max} in [32] $= 10A = 1.4I_{rated}$). The sixth control strategy in [33] with the zero power oscillations can be obtained when implementing the maximum voltage limit. Also, the same control objective in [34] can operate at zero power oscillations. In a practical system, however, the capability of maximizing power delivery should be considered depending on both the volt-ampere sizing of DVR and the different grid scenarios.

In addition, the control strategy based on the presented identification tool is the kernel to realize the adjustable power dispatches. The gradual transition from one power delivery level to another is described accurately by these preset parameter distributions, and it allows to show the power dispatch trend embedded in the presented identification tool. Also, this identification tool has been chosen as the operational mechanism to implement all the tests when the current references with the combination of two power deliveries are determined by setting the proper values of two control parameters. It is possible to simultaneously regulate the active power to a preset point and correct the deviation of the reactive power, and vice versa.

V. Conclusion

The application of elliptical compensation has provided flexible controllability of power support schemes. Also, a new identification tool has been described through the selection of two control parameters. The smooth transition state during changes in different power deliveries and the elimination of active and reactive power oscillations can be realized by setting useful values of control parameters. Meanwhile, the proposed control strategy displays a pretty better dynamic behavior, as can be seen from the identification approach. Detailed theoretical analysis and experimental verification have been achieved. Finally, application examples have been allowed to illustrate the feasibility of the given control algorithm.

Acknowledgment

This work was supported by the China Postdoctoral Science Foundation under Project 2020M681093, and also supported by the Shenzhen Basic Research Project under grant JCYJ20180306172056738.

References

[1] C. Tu, Q. Guo, F. Jiang, H. Wang, and Z. Shuai, “A comprehensive study to mitigate voltage sags and phase jumps using a dynamic voltage restorer,” *IEEE Journal of Emerging and Selected Topics in Power Electronics*, vol. 8, no. 2, pp. 1490–1502, 2020.

[2] A. P. Torres, P. Roncero-Sanchez, and V. F. Batlle, “A two degrees of freedom resonant control scheme for voltage-sag compensation in dynamic voltage restorers,” *IEEE Transactions on Power Electronics*, vol. 33, no. 6, pp. 4852–4867, 2017.

[3] S. Priyavarthini, A. C. Kathiresan, C. Nagamani, and S. I. Ganesan, “Pv-fed dvr for simultaneous real power injection and sag/swell mitigation in a wind farm,” *IET Power Electronics*, vol. 11, no. 14, pp. 2385–2395, 2018.

[4] Y. Zhang and C. Qu, “Direct power control of a pulse width modulation rectifier using space vector modulation under unbalanced grid voltages,” *IEEE Transactions on Power Electronics*, vol. 30, no. 10, pp. 5892–5901, 2014.

[5] C. Meyer, R. W. De Doncker, Y. W. Li, and F. Blaabjerg, "Optimized control strategy for a medium-voltage dvr¡ªtheoretical investigations and experimental results," *IEEE Transactions on Power Electronics*, vol. 23, no. 6, pp. 2746–2754, 2008.

[6] F. Jiang, C. Tu, Q. Guo, Z. Shuai, X. He, and J. He, "Dual-functional dynamic voltage restorer to limit fault current," *IEEE Transactions on Industrial Electronics*, vol. 66, no. 7, pp. 5300–5309, 2019.

[7] A. dos Santos, T. Rosa, and M. T. C. de Barros, "Stochastic characterization of voltage sag occurrence based on field data," *IEEE Transactions on Power Delivery*, vol. 34, no. 2, pp. 496–504, 2018.

[8] J. L. Sosa, M. Castilla, J. Miret, J. Matas, and Y. Al-Turki, "Control strategy to maximize the power capability of pv three-phase inverters during voltage sags," *IEEE Transactions on Power Electronics*, vol. 31, no. 4, pp. 3314–3323, 2015.

[9] S. Choi, J. Li, and D. M. Vilathgamuwa, "A generalized voltage compensation strategy for mitigating the impacts of voltage sags/swells," *IEEE Transactions on Power Delivery*, vol. 20, no. 3, pp. 2289–2297, 2005.

[10] M. Castilla, J. Miret, A. Camacho, J. Matas, and L. G. de Vicuña, "Voltage support control strategies for static synchronous compensators under unbalanced voltage sags," *IEEE Transactions on Industrial Electronics*, vol. 61, no. 2, pp. 808–820, 2013.

[11] J. Wang, Y. Xing, H. Wu, and T. Yang, "A novel dual-dc-port dynamic voltage restorer with reduced-rating integrated dc¨cdc converter for wide-range voltage sag compensation," *IEEE Transactions on Power Electronics*, vol. 34, no. 8, pp. 7437–7449, 2019.

[12] A. Parreñno Torres, P. Roncero-Sñanchez, J. Vñazquez, F. J. Lñopez-Alcolea, and E. J. Molina-Martñinez, "A discrete-time control method for fast transient voltage-sag compensation in dvr," *IEEE Access*, vol. 7, pp. 170 564–170 577, 2019.

[13] V. Valouch, M. Bejvl, P. Šimek, and J. Škramlīk, "Power control of grid-connected converters under unbalanced voltage conditions," *IEEE Transactions on Industrial Electronics*, vol. 62, no. 7, pp. 4241–4248, 2014.

[14] M. Pradhan and M. K. Mishra, "Dual p- q theory based energy-optimized dynamic voltage restorer for power quality improvement in a distribution system," *IEEE Transactions on Industrial Electronics*, vol. 66, no. 4, pp. 2946–2955, 2019.

[15] T. A. Naidu, S. R. Arya, and R. Maurya, "Multiobjective dynamic voltage restorer with modified epll control and optimized pi-controller gains," *IEEE Transactions on Power Electronics*, vol. 34, no. 3, pp. 2181–2192, 2018.

[16] Z. Zheng, X. Xiao, C. Huang, and C. Li, "Enhancing transient voltage quality in a distribution power system with smes-based dvr and sfcl," *IEEE Transactions on Applied Superconductivity*, vol. 29, no. 2, pp. 1–5, 2018.

[17] A. Camacho, M. Castilla, J. Miret, R. Guzman, and A. Borrell, "Reactive power control for distributed generation power plants to comply with voltage limits during grid faults," *IEEE Transactions on Power Electronics*, vol. 29, no. 11, pp. 6224–6234, 2014.

[18] A. Camacho, M. Castilla, J. Miret, L. G. de Vicuña, and R. Guzman, "Positive and negative sequence control strategies to maximize the voltage support in resistive¨cinductive grids during grid faults," *IEEE Transactions on Power Electronics*, vol. 33, no. 6, pp. 5362–5373, 2018.

[19] A. Camacho, M. Castilla, J. Miret, L. G. de Vicuña, and G. L. M. Andrés, "Control strategy for distribution generation inverters to maximize the voltage support in the lowest phase during voltage sags," *IEEE Transactions on Industrial Electronics*, vol. 65, no. 3, pp. 2346–2355, 2017.

[20] A. Karthikeyan, D. G. A. Krishna, S. Kumar, B. V. Perumal, and S. Mishra, "Dual role cdsc-based dual vector control for effective operation of dvr with harmonic mitigation," *IEEE Transactions on Industrial Electronics*, vol. 66, no. 1, pp. 4–13, 2019.

[21] X. Wang, F. Blaabjerg, and P. C. Loh, "Virtual rc damping of lcl-filtered voltage source converters with extended selective harmonic compensation," *IEEE Transactions on Power Electronics*, vol. 30, no. 9, pp. 4726–4737, 2015.

[22] E. Babaei, M. F. Kangarlu, and M. Sabahi, "Dynamic voltage restorer based on multilevel inverter with adjustable dc-link voltage," *IET Power Electronics*, vol. 7, no. 3, pp. 576–590, 2014.

[23] E. K. K. Sng, S. S. Choi, and D. M. Vilathgamuwa, "Analysis of series compensation and dc-link voltage controls of a transformerless self-charging dynamic voltage restorer," *IEEE Transactions on Power Delivery*, vol. 19, no. 3, pp. 1511–1518, 2004.

[24] C. Lam, M. Wong, and Y. Han, "Voltage swell and overvoltage compensation with unidirectional power flow controlled dynamic voltage restorer," *IEEE Transactions on Power Delivery*, vol. 23, no. 4, pp. 2513–2521, 2008.

[25] E. A. Awad, E. A. Badran, and F. H. Youssef, "Mitigation of switching overvoltages in microgrids based on svc and supercapacitor," *IET Generation, Transmission Distribution*, vol. 12, no. 2, pp. 355–362, 2018.

[26] X. Lin, Z. Liang, Y. Zheng, Y. Lin, and Y. Kang, "A current limiting strategy with parallel virtual impedance for three-phase three-leg inverter under asymmetrical short-circuit fault to improve the controllable capability of fault currents," *IEEE Transactions on Power Electronics*, vol. 34, no. 8, pp. 8138–8149, 2019.

[27] W. Liu, F. Blaabjerg, D. Zhou, and S. Chou, "Modified instantaneous power control with phase compensation and current-limited function under unbalanced grid faults," *IEEE Journal of Emerging and Selected Topics in Power Electronics*, pp. 1–1, 2020.

[28] J. Miret, M. Castilla, A. Camacho, L. G. d. Vicuña, and J. Matas, "Control scheme for photovoltaic three-phase inverters to minimize peak currents during unbalanced grid-voltage sags," *IEEE Transactions on Power Electronics*, vol. 27, no. 10, pp. 4262–4271, 2012.

[29] M. Castilla, J. Miret, J. L. Sosa, J. Matas, and L. G. d. Vicuña, "Grid-fault control scheme for three-phase photovoltaic inverters with adjustable power quality characteristics," *IEEE Transactions on Power Electronics*, vol. 25, no. 12, pp. 2930–2940, 2010.

[30] A. Camacho, M. Castilla, J. Miret, J. C. Vasquez, and E. Alarcon-Gallo, "Flexible voltage support control for three-phase distributed generation inverters under grid fault," *IEEE Transactions on Industrial Electronics*, vol. 60, no. 4, pp. 1429–1441, 2013.

[31] X. Guo, W. Liu, and Z. Lu, "Flexible power regulation and current-limited control of the grid-connected inverter under unbalanced grid voltage faults," *IEEE Transactions on Industrial Electronics*, vol. 64, no. 9, pp. 7425–7432, 2017.

[32] A. Camacho, M. Castilla, J. Miret, A. Borrell, and L. G. de Vicuña, "Active and reactive power strategies with peak current limitation for distributed generation inverters during unbalanced grid faults," *IEEE Transactions on Industrial Electronics*, vol. 62, no. 3, pp. 1515–1525, 2014.

[33] J. Miret, A. Camacho, M. Castilla, L. G. de Vicuña, and J. Matas, "Control scheme with voltage support capability for distributed generation inverters under voltage sags," *IEEE Transactions on Power Electronics*, vol. 28, DOI 10.1109/TPEL.2013.2246190, no. 11, pp. 5252–5262, 2013.

[34] J. Jia, G. Yang, and A. H. Nielsen, "A review on grid-connected converter control for short-circuit power provision under grid unbalanced faults," *IEEE Transactions on Power Delivery*, vol. 33, no. 2, pp. 649–661, 2017.

[35] P. Li, L. Xie, J. Han, S. Pang, and P. Li, "A new voltage compensation philosophy for dynamic voltage restorer to mitigate voltage sags using three-phase voltage ellipse parameters," *IEEE Transactions on Power Electronics*, vol. 33, no. 2, pp. 1154–1166, 2017.

[36] P. Li, L. Xie, J. Han, S. Pang, and P. Li, "New decentralized control scheme for a dynamic voltage restorer based on the elliptical trajectory compensation," *IEEE Transactions on Industrial Electronics*, vol. 64, no. 8, pp. 6484–6495, 2017.

[37] M. H. Bollen, "Understanding power quality problems: Voltage sags and interruptions," *NJ:Wiley-IEEE Press,2000*.

[38] "Ieee recommended practice for monitoring electric power quality," *IEEE Std 1159-2019 (Revision of IEEE Std 1159-2009)*, pp. 1–98, 2019.

[39] W. E. Brumsickle, R. S. Schneider, G. A. Luckjiff, D. M. Divan, and M. F. McGranaghan, "Dynamic sag correctors: cost-effective industrial power line conditioning," *IEEE Transactions on Industry Applications*, vol. 37, no. 1, pp. 212–217, 2001.

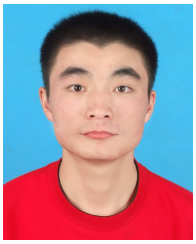

Peng Li was born in Henan, China, on September 29, 1985. He graduated from the Henan Mechanical and Electrical Engineering College in Electrical Power Systems and Automation, Xinxiang and received the master degree in Electrical Engineering from the North China University of Water Resources and Electric Power, Zhengzhou in 2008 and 2013, respectively, and the PhD. degree in electrical engineering from the Northwestern Polytechnical University, Xi'an Shaanxi, China, 2018. He is currently working toward the Postdoc in Harbin Institute of Technology (Shenzhen), China.

His current reseach includes the application of soft computing techniques to power system, distributed generation, power quality and reliability.

Yi Wang was born in Heilongjiang, China, in 1966. He received the B.E. degree from Xi?an Technological University, Xi?an, China in 1988. He obtained his M.S. and Ph.D. degrees from Harbin Institute of Technology, Harbin, China, in 1996, and 2002, respectively. Since 2009, he has been a Professor at Shenzhen Graduate School, Harbin Institute of Technology, Shenzhen, China.

His research interests include soft-switching techniques, power converters control, digital control techniques for power electronic circuits, and renewable energy systems

Mehdi Savaghebi (S'06-M'15-SM'15) received the B.Sc. degree from University of Tehran, Iran, in 2004 and the M.Sc. and Ph.D. degrees with highest honors from Iran University of Science and Technology, Tehran, Iran in 2006 and 2012, respectively, all in Electrical Engineering. From 2014 to 2017, he was a Postdoc Fellow in the Department of Energy Technology, Aalborg University where he was an Associate Professor for 2017-2018. Currently, he is an Associate Professor with Electrical Engineering Section, the Mads Clausen Institute, University of Southern Denmark, Odense, Denmark.

His main research interests include distributed generation systems, microgrids, power quality and protection of electrical systems, UPS and smart metering. Dr. Savaghebi has been a Guest Editor of Special Issue on Power Quality in Smart Grids- IEEE Transactions on Smart Grid, Special Issue on Power Quality and Protection in Renewable Energy Systems and Microgrids- IET Renewable Power Generation and Special Issue on Uninterruptible Power Supplies- MDPI Sustainability Journal. He was a member of Task Force on Microgrid Stability Analysis and Modeling, IEEE Power and Energy Society. He is an Associate Editor of IEEE Access, Editor of MDPI Sustainability journal and a member of Technical Committee of Renewable Energy Systems, IEEE Industrial Electronics Society

Jinghang Lu (S'14-M'18) received the B.Sc. degree in electrical engineering from Harbin Institute of Technology, China, in 2009, two M.Sc. degrees both in electrical engineering from Harbin Institute of Technology, China, in 2011, and University of Alberta, Canada, in 2014, respectively, and the Ph.D. degree in Power Electronics from Aalborg University, Aalborg, Denmark, in 2018. From 2018 to 2019, He was a Research Fellow in Nanyang Technological University, Singapore. Currently, he is an Assistant Professor with Harbin Institute of Technology (Shenzhen), Shenzhen, China.

His research interests include uninterruptible power supply, microgrid, and control of power converters.

Xuewei Pan (S'12-M'16) received the B.E. degree in Electronic Engineering from University of Electronic Science and Technology of China (UESTC), Chengdu, China in 2011. He obtained his Ph.D. degree in the area of Power Electronics at Electrical and Computer Engineering, National University of Singapore in 2015. He worked as a research fellow in Energy Research Institute @ NTU (ERI@N) from July 2014 to September 2016 in Singapore. Currently He is an Associate Professor in Harbin Institute of Technology, Shenzhen, China.

His research interests include distributed generation, renewable integration, micro-grid energy system, soft-switching methods and modulation techniques for high frequency power conversion for renewable energy.

Frede Blaabjerg (S'86-M'88-SM'97-F'03) was with ABB-Scandia, Randers, Denmark, from 1987 to 1988. From 1988 to 1992, he got the PhD degree in Electrical Engineering at Aalborg University in 1995. He became an Assistant Professor in 1992, an Associate Professor in 1996, and a Full Professor of power electronics and drives in 1998. From 2017 he became a Villum Investigator. He is honoris causa at University Politehnica Timisoara (UPT), Romania and Tallinn Technical University (TTU) in Estonia.

His current research interests include power electronics and its applications such as in wind turbines, PV systems, reliability, harmonics and adjustable speed drives. He has published more than 600 journal papers in the fields of power electronics and its applications. He is the co-author of four monographs and editor of ten books in power electronics and its applications.

He has received 32 IEEE Prize Paper Awards, the IEEE PELS Distinguished Service Award in 2009, the EPE-PEMC Council Award in 2010, the IEEE William E. Newell Power Electronics Award 2014, the Villum Kann Rasmussen Research Award 2014, the Global Energy Prize in 2019 and the 2020 IEEE Edison Medal. He was the Editor-in-Chief of the IEEE TRANSACTIONS ON POWER ELECTRONICS from 2006 to 2012. He has been Distinguished Lecturer for the IEEE Power Electronics Society from 2005 to 2007 and for the IEEE Industry Applications Society from 2010 to 2011 as well as 2017 to 2018. In 2019-2020 he serves a President of IEEE Power Electronics Society. He is Vice-President of the Danish Academy of Technical Sciences too. He is nominated in 2014-2019 by Thomson Reuters to be between the most 250 cited researchers in Engineering in the world.